

# Supplementary Information

## Light-activated shape morphing and light-tracking materials using biopolymer-based programmable photonic nanostructures

Yu Wang<sup>1,2,9</sup>, Meng Li<sup>1,2,9</sup>, Jan-Kai Chang<sup>3</sup>, Daniele Aurelio<sup>4</sup>, Wenyi Li<sup>1,2</sup>, Beom Joon Kim<sup>1,2</sup>, Jae Hwan Kim<sup>3</sup>, Marco Liscidini<sup>4</sup>, John A. Rogers<sup>3,5</sup> and Fiorenzo G. Omenetto<sup>1,2,6,7,8\*</sup>

<sup>1</sup>SilkLab, Suite 4875, 200 Boston Avenue, Tufts University, Medford, MA 02155, USA.

<sup>2</sup>Department of Biomedical Engineering, Tufts University, Medford, MA 02155, USA.

<sup>3</sup>Center for Bio-Integrated Electronics, Northwestern University, Evanston, IL 60208, USA.

<sup>4</sup>Dipartimento di Fisica, Università degli Studi di Pavia, via Bassi 6, 27100 Pavia, Italy.

<sup>5</sup>Departments of Materials Science and Engineering, Biomedical Engineering, Neurological Surgery, Chemistry, Mechanical Engineering, Electrical Engineering and Computer Science, and Simpson Querrey Institute for BioNanotechnology, Northwestern University, Evanston, IL 60208, USA.

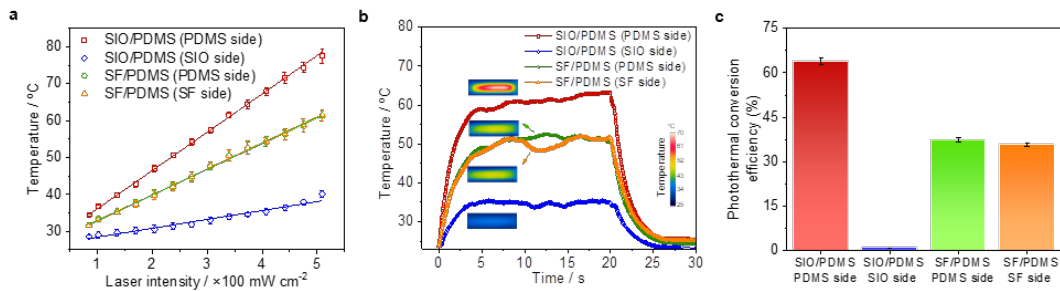
<sup>6</sup>Department of Physics, Tufts University, Medford, MA 02155, USA.

<sup>7</sup>Department of Electrical Engineering, Tufts University, Medford, MA 02155, USA.

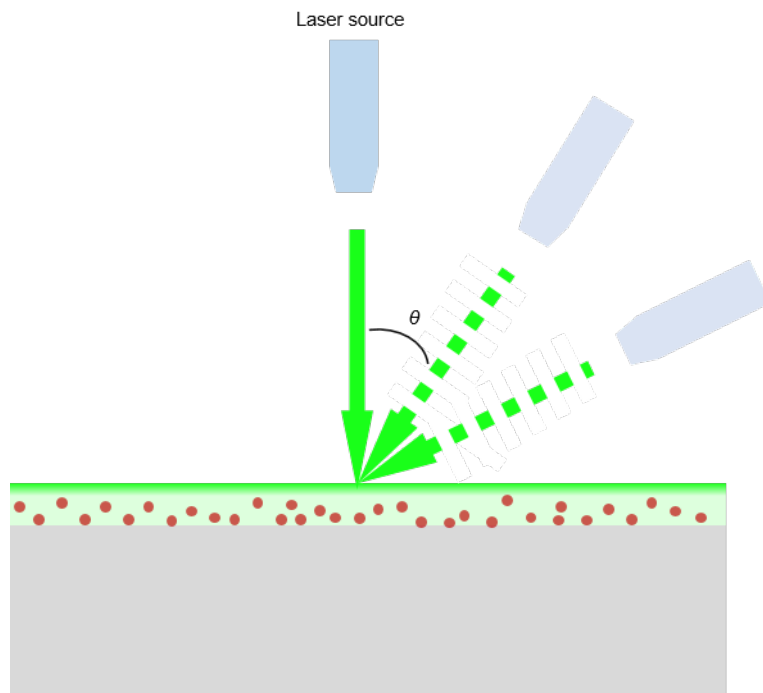
<sup>8</sup>Laboratory for Living Devices, Tufts University, Medford, MA 02155, USA.

<sup>9</sup>These authors contributed equally to this work: Yu Wang, Meng Li.

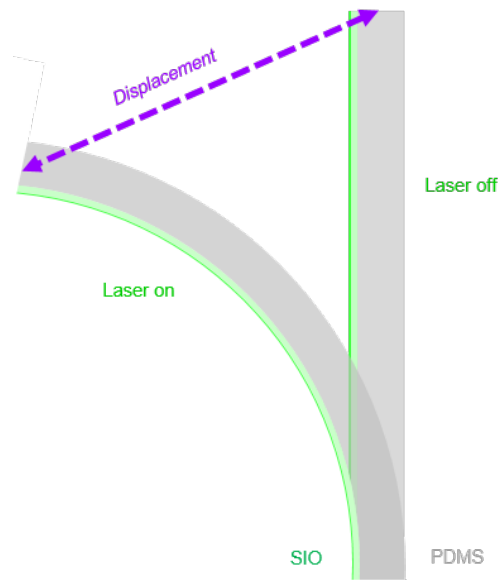
\*Corresponding author. E-mail: [Fiorenzo.Omenetto@tufts.edu](mailto:Fiorenzo.Omenetto@tufts.edu)



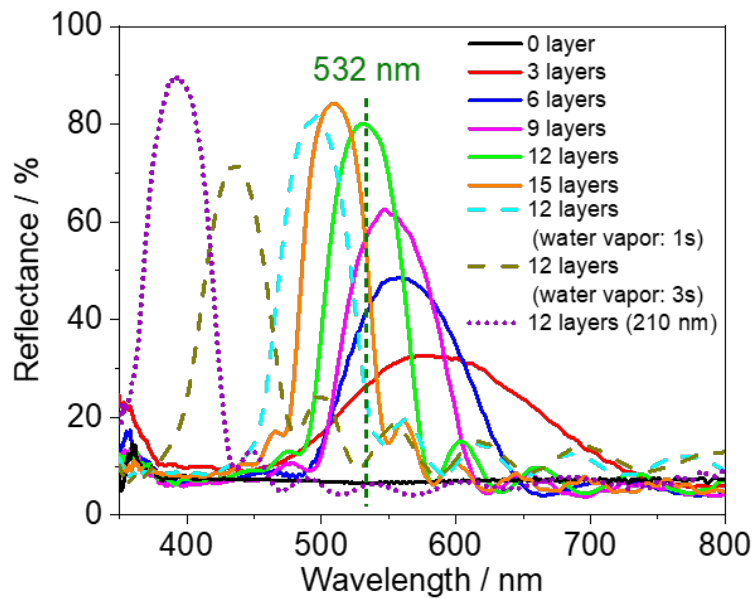
**Supplementary Fig. 1. Photothermal conversion of bilayer films.** **a**, Measured temperature increases as a function of laser irradiance. SIO/PDMS sample is the most and least heated when PDMS side and SIO side illumination are performed, respectively, while the SF/PDMS sample shows intermediate values and no dependence on the illumination direction. **b**, Measured temperature increases as a function of laser illumination time ( $I = 350 \text{ mW cm}^{-2}$ ). The temperature of SIO/PDMS sample with PDMS side illumination increases rapidly from room temperature ( $\sim 25 \text{ }^\circ\text{C}$ ) to a maximum temperature of  $\sim 63 \text{ }^\circ\text{C}$ , but it slowly rises to  $\sim 30 \text{ }^\circ\text{C}$  for SIO side illumination. The temperature of SF/PDMS film increases to  $\sim 51 \text{ }^\circ\text{C}$  at a moderate speed. Insets show the corresponding Infrared images after laser irradiation for 20 s. **c**, The calculated photothermal efficiency of the bilayer films. The photo-thermal conversion efficiency  $\eta$  reaches  $63.83\% \pm 1.1\%$  for SIO/PDMS film with PDPS side illumination, while it is only  $0.80\% \pm 0.06\%$  when SIO side is illuminated. The SF/PDMS film has similar and middle  $\eta$  values for both PDMS side ( $37.30\% \pm 0.7\%$ ) and SF side ( $35.64\% \pm 0.5\%$ ) illumination. Error bars denote the standard deviation of the measurements ( $n = 5$ ).



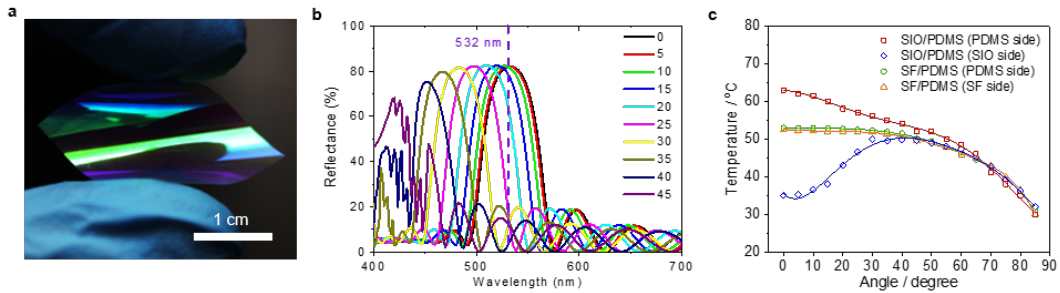
**Supplementary Fig. 2. Schematic illustration of the bilayer sample illuminated at different angles.  $\theta$  is defined as incident angle of laser beam.**



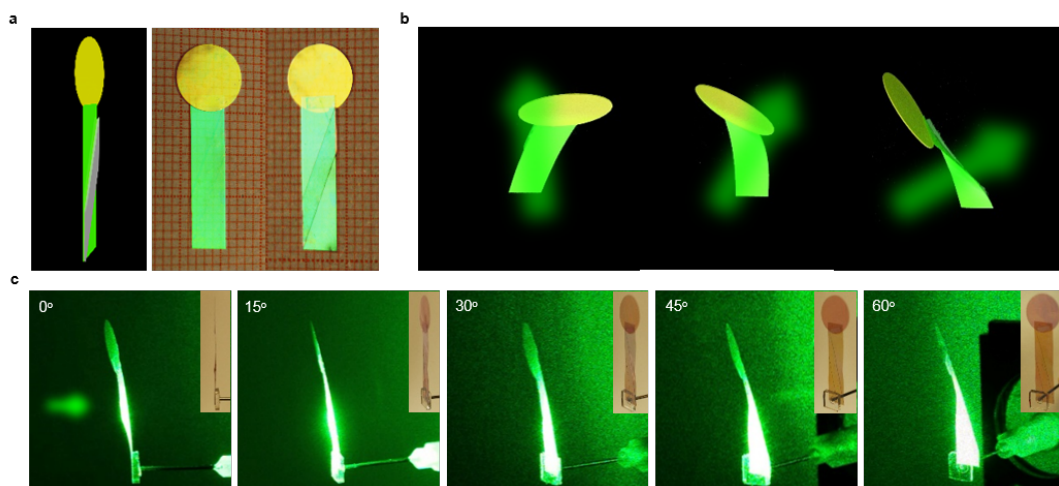
**Supplementary Fig. 3. Schematic illustration of the calculation of displacement.**  
The displacement is defined as the straight-line distance of the tip traveled.



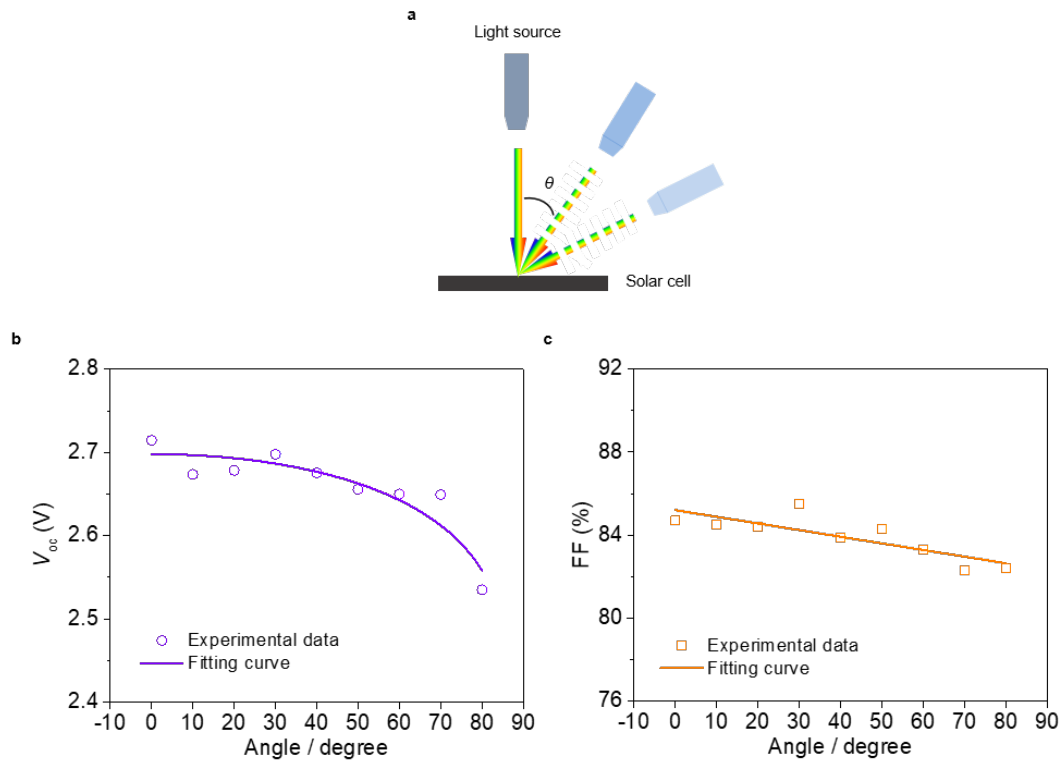
**Supplementary Fig. 4. Reflectance spectra of photonic bilayer films with different photonic nanostructures.** Different reflectance properties are generated by controlling layer numbers or lattice constants of SIOs or by reconfiguring the photonic lattices through contact-less water vapor exposure. The blueshift of the stop-band with the increase of the number of layers results from the shrinkage of the silk nanostructures in the out-of-plane vertical direction during immersion in toluene (to remove the template) and/or drying (to remove toluene). Such shrinkage occurred because silk in its amorphous configuration was used.



**Supplementary Fig. 5. Angle-dependent reflection and heating.** **a**, Photograph of a bent green colored photonic bilayer film showing different structural colors at different parts. **b**, Simulated reflectance spectra of green colored photonic bilayer film at different incident angles. The stop-band peak is gradually blue-shifted with the increase of incident angle, leading to the gradual decrease of reflection intensity at 532 nm (laser wavelength). **c**, Measured temperature as a function of laser illumination angle ( $I = 350 \text{ mW cm}^{-2}$ ). The temperature of the SIO/PDMS bilayer decreases gradually with angle for PDMS side illumination, while it increases first and then decreases if SIO side is illuminated. By comparison, the temperature of SF/PDMS bilayer decreases gradually regardless of illumination direction. Error bars denote the standard deviation of the measurements ( $n = 5$ ).

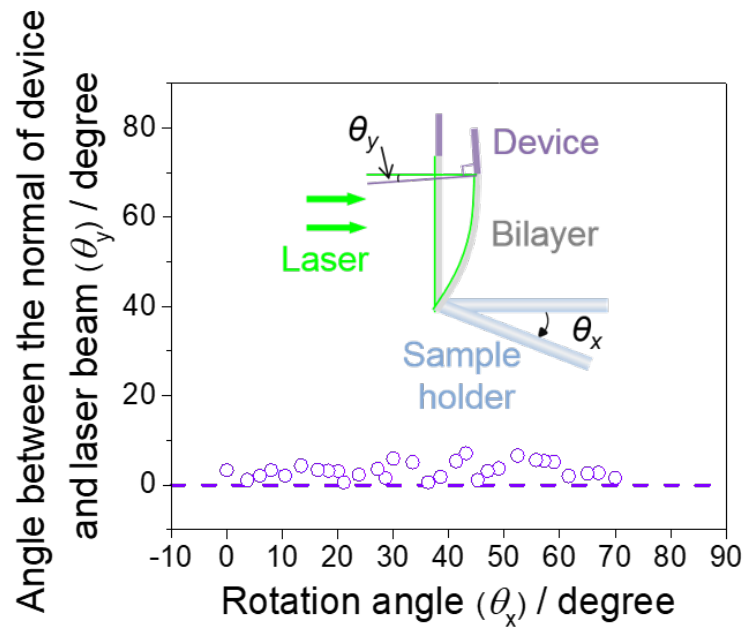


**Supplementary Fig. 6. Phototropic twisting motion.** **a**, Schematic and photograph of a lollipop-like geometry with the illustration of phototropic twisting movement. **b**, **c**, Schematics (**b**) and images (**c**) showing different deformation states of the lollipop-like geometry with different illumination angles. The sample tracks the light source continuously with the continuous twisting movement. Insets in (**c**) indicate the initial state of the sample at each angle before illumination.

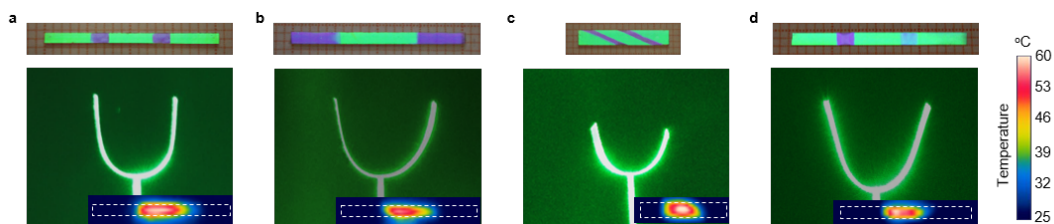


**Supplementary Fig. 7. Performance of a microscale 3J solar  $\mu$ -cell. a**, Schematic showing the definition of illumination angle ( $\theta$ ). **b**, **c**, Measured open-circuit voltage  $V_{oc}$  (**b**), and fill factor  $FF$  (**c**) as a function of incident angle.

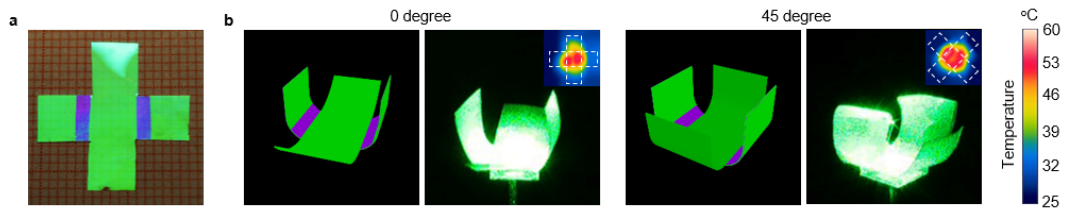




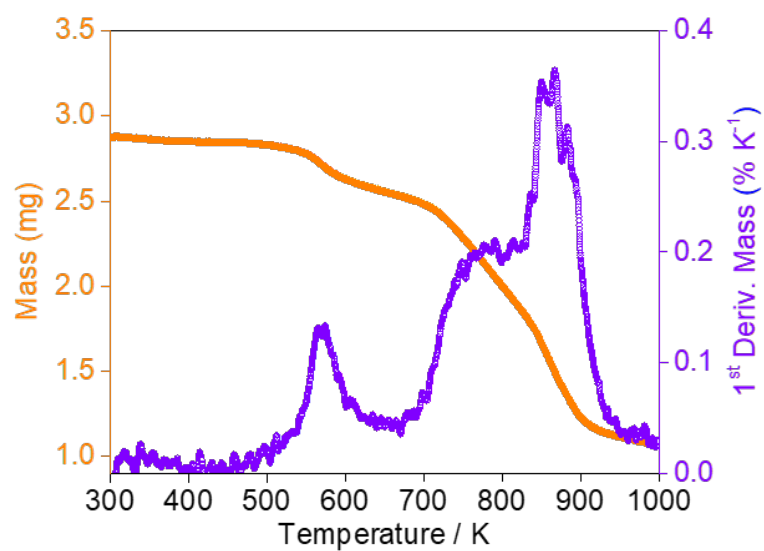
**Supplementary Fig. 8.** Angle between the normal of solar cells' substrate and laser beam ( $\theta_y$ ) as a function of rotation angle of the sample ( $\theta_x$ ). The angle between the device substrate and the laser beam almost keeps constant with the increase of rotation angle. The dashed line represents the angle of  $\theta_y = 0^\circ$ . Inset is the schematic of the definitions of  $\theta_x$  and  $\theta_y$ .



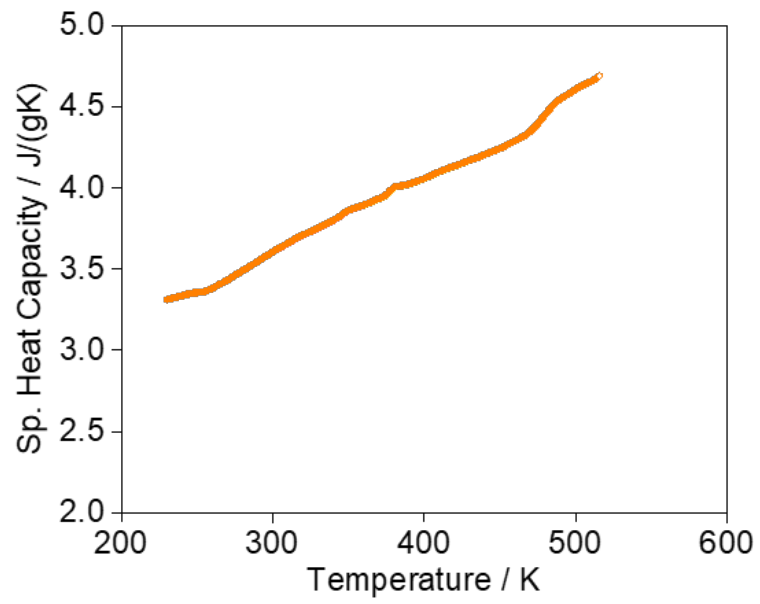
**Supplementary Fig. 9 Photographs showing the pattern designs and the corresponding motion modes under laser illumination at 45°. a-d, Only bending is generated for all designs. Insets in (a-d) indicate the associated infrared images of the patterned strips under laser irradiation with dashed line outlining the edge of the sample before laser irradiation.**



**Supplementary Fig. 10. A self-folding box.** **a**, Photograph of a cross-shaped piece of photonic bilayer film. **b**, Schematics and images showing the self-folding behavior under laser illumination at  $0^\circ$  and  $45^\circ$  from SIO side. Insets indicate the associated infrared images of the self-folding box under laser irradiation with dashed line outlining the edge of the sample before laser irradiation.



**Supplementary Fig. 11. Thermal gravimetric results for photonic bilayer film.** Water content in SF sample is ~0.70 wt% from mass loss below 373 K. The thermal degradation onset temperature is 573 K.



**Supplementary Fig. 12.** Specific heat capacity result for photonic bilayer film.